**Supporting information**

# Anisotropic layer-by-layer carbon nanotubes/boron nitride/rubber composite and its application in electromagnetic shielding

Yanhu Zhan[1], Emanuele Lago[2,3], Chiara Santillo[4], Antonio Esaú Del Río Castillo[2], Shuai Hao[5], Giovanna G. Buonocore[4], Zhenming Chen[6], Hesheng Xia[5], Marino Lavorgna[4*], Francesco Bonaccorso[2,7]

1. School of Materials Science and Engineering, Liaocheng University, Liaocheng 252000, China

2. Graphene Labs, Italian Institute of Technology, via Morego 30, 16163 Genoa, Italy

3. Dipartimento di Chimica e Chimica Industriale, Università degli Studi di Genova, via Dodecaneso 31, 16146 Genoa, Italy

4. Institute of Polymers, Composites and Biomaterials, National Research Council, P.le Fermi, 1-80055 Portici, NA, Italy.

5. State Key Laboratory of Polymer Materials Engineering, Polymer Research Institute, Sichuan University, Chengdu 610065, China

6. Guangxi Key Laboratory of Calcium Carbonate Resources Comprehensive Utilization, Hezhou University, Hezhou, City 542899, China.

7. BeDimensional S.p.a. Via Albisola 121, Genova 16163, Italy

* E-mail address: marino.lavorgna@cnr.it

**1. *h*BN and few-layers graphene characterization.**

1.1 Transmission electron microscopy. The *h*BN and the graphene samples are diluted 1:50, in N-methyl-2-pyrrolidone, and stored under vacuum at room temperature. TEM images are taken by using a JEOL JEM-1011 transmission electron microscope, operated at an acceleration voltage of 100 kV.

1.2 Atomic Force microscopy. The dispersions are diluted 1:30 in NMP. 100 mL of the dilutions are drop-cast onto $Si/SiO_2$ wafers and dried at 50 °C overnight. AFM images are acquired with a Bruker Innova AFM in tapping mode using silicon probes (frequency = 300 kHz, spring constant = 40 N $m^{-1}$). The thickness statistics are analysed by measuring B100 flakes from the AFM images. Statistical distributions are fitted with log-normal curves. Statistical analyses are performed in WSxM Beta 4.0 software.

1.3 Raman spectroscopy. The as-prepared dispersions are diluted 1:30 in NMP and drop cast onto a Si wafer (LDB Technologies Ltd) covered with 300 nm thermally grown $SiO_2$. The bulk materials are analysed in the powder form. Raman measurements are carried out by using a Renishaw inVia spectrometer using a 50x objective (numerical aperture 0.75), and a laser with a wavelength of 514.5 nm with an incident power of mW. A total of 30 points per sample are measured to perform the statistical analysis. OriginPro 2016 is used to perform the deconvolution and statistics.

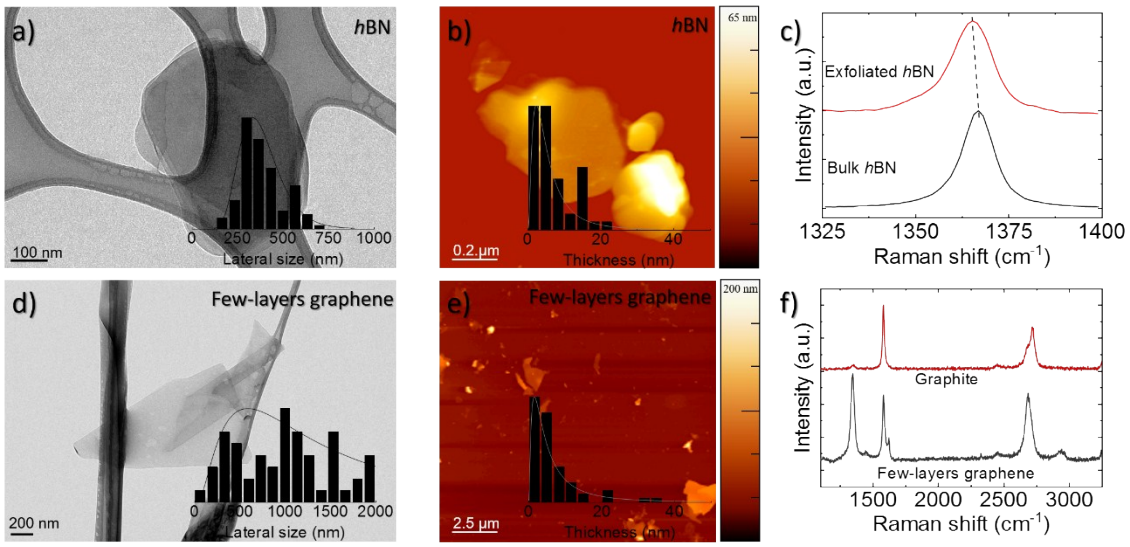


**Figure S1**. Characterisation of the exfoliated *h*BN and graphite. a) A TEM image of an exfoliated *h*BN flake, the inset shows the size distribution with a mode of 360 nm. b) AFM image of exfoliated *h*BN flakes, the inset shows the thickness distribution with a mode of 2.4 nm. c) Raman spectroscopy comparing the characteristic $E_{2g}$ peak

of bulk and exfoliated *h*BN. d) The TEM image of exfoliated few-layers graphene flakes, the inset shows the size distribution with a mode of 460 nm. b) AFM image of exfoliated flakes, the inset shows the thickness distribution with a mode of 1.6 nm. c) Raman spectroscopy comparing the characteristic D, G and 2D bands of bulk and exfoliated graphite flakes.

## 2 Polymer composites characterization.

**Table S1**. The experimental formula of composites latex for realizing the CNTs and *h*BN composite layers, the mass of HMR 10 latex was 4.23 g and $H_2O$ was 38 g.

| Filler* content (phr) | Filler* content (wt%) | Filler* (g) | CTAB (g) |
|---|---|---|---|
| 2 | 1.96 | 0.05 | 0.05 |
| 4 | 3.85 | 0.1 | 0.1 |
| 6 | 5.66 | 0.15 | 0.15 |
| 8 | 7.41 | 0.2 | 0.2 |
| 12 | 10.71 | 0.3 | 0.3 |
| 16 | 13.79 | 0.4 | 0.4 |

*Filler refers to CNTs and *h*BN

**Table** S2. Thermal and electrical conductivity and EMI SE of layered composites with graphene having thickness of 1.4 mm.

| | Thermal conductivity ($Wm^{-1}K^{-1}$) | Electrical conductivity ($S\ cm^{-1}$) | EMI SE (dB) |
|---|---|---|---|
| 8-R(graphene$_4$C$_4$)B$_8$ | 0.33 | 0.234 | 15.02 |
| 8-R(graphene$_8$)B$_8$ | 0.35 | $3.98\times10^{-5}$ | 11.57 |

**Table S3**. EMI SE in 8.2-12.4 GHz range for the presented NR/CNT composites and

the layered rubber composites prepared in this work.

| Sample | Thickness (mm) | CNT content (wt%) | SE (dB) | specific EMI SE (dB $mm^{-1}$) | Ref. |
|---|---|---|---|---|---|
| NR/$CNT_{6.40}$ foam | 1.3 | 6.40 | 33.74 | 25.95 | [S1] |
| CNT/NR | 1.5 | 5.0 | 33.3 | 22.2 | [S2] |
| SBR/CNT | 5 | 9.09 | 35.06 | 7.01 | [S3] |
| BR/CNT | 1 | 7.41 | 13 | 13 | [S4] |
| NR/ENR/CB | 4 | 23.08 | 23.58 | 5.90 | [S5] |
| TPNR/$Fe_3O_4$ | 9 | 12 | 25.52 | 2.84 | [S6] |
| NR/CB/silica | 2.83 | 41.18 | 16.06 | 5.67 | [S7] |
| tire rubber/CNT | 2.6 | 2 (+13.1 CB) | 36.8 | 14.15 | [S8] |
| NR/$Fe_3O_4$@graphene | 1.6 | 4.50 (graphene) +20.48 ($Fe_3O_4$) | 32.9 | 20.56 | [S9] |
| 8-$RC_8B_{12}$ | 1.4 | 7.4 (+10.7 wt% *h*BN) | 28.87[#]<br>31.38[##] | 20.62[#]<br>22.41[##] | This work |
| 8-$RC_8B_{16}$ | 1.4 | 7.4 (+13.8 wt% *h*BN) | 29.93[#]<br>32.52[##] | 21.38[#]<br>23.23[##] | This work |

[#] electromagnetic waves entering from NR/CNT layer
[##] electromagnetic waves entering from NR/*h*BN layer

**Table S4.** The electric heating behaviour of polymer-based composites with lengths of 10 mm and wide of 3 mm.

| Sample | Filler content | Thickness (mm) | Potential (V) | Steady-state temperature (°C) | Ref |
|---|---|---|---|---|---|
| Epoxy/graphene | 10 wt% | 0.1 | 30 | 126 | [S10] |
| Epoxy/graphene/CNT | 10 wt% | 0.1 | 20 | 160 | [S11] |
| Epoxy/graphene | 10wt% | 0.1 | 20 | 40 | [S11] |
| PDMS/CNT/graphene | 10wt% | - | 20 | ~55 | [S12] |
| PDMS/graphene-90/10 | 10wt% | - | 20 | ~25 | [S12] |
| 8-$RC_4B_8$ | 4phr CNT 8phr hBN | 1.4 | 5 | 165.4 | This work |
| 8-$RC_8B_{12}$ | 8phr CNT 12phr hBN | 1.4 | 2.5 | 103.3 | This work |

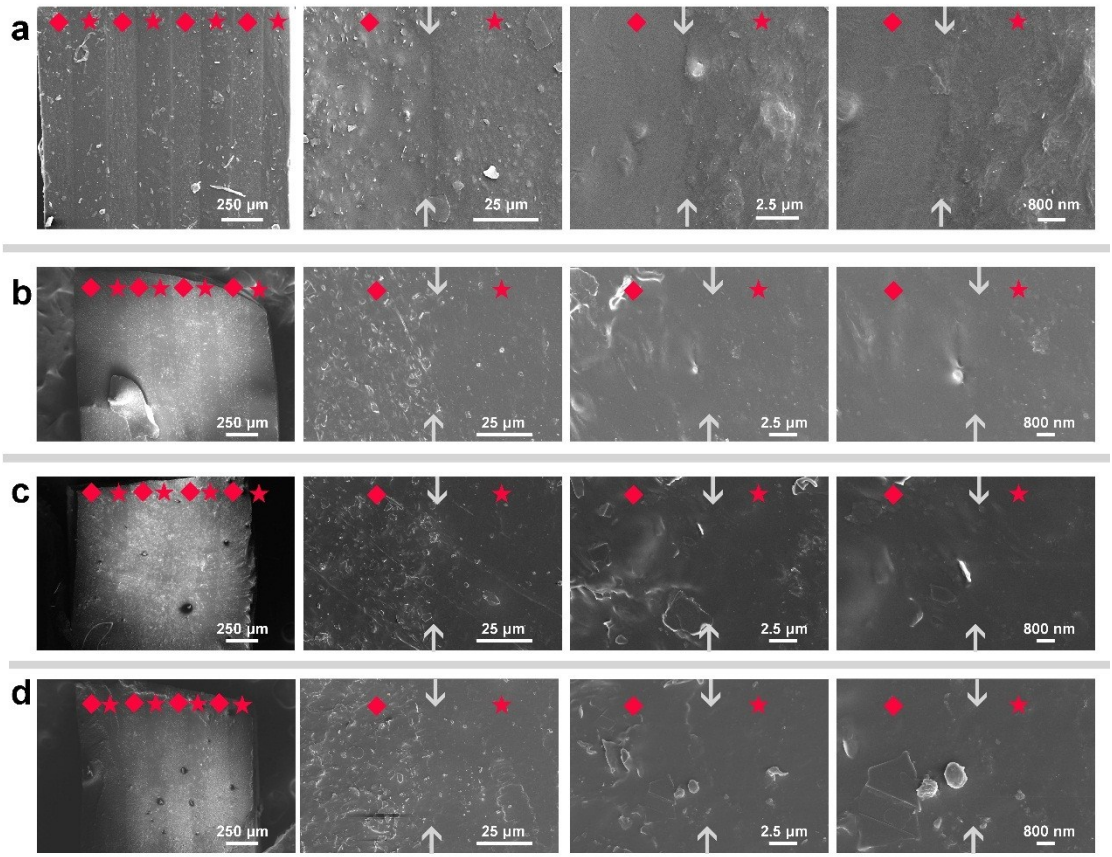


**Figure S2.** SEM image of 8-$RC_8B_{12}$ sample (a) and 8-$RC_2B_8$ sample before (b) and after (c) bending cycles; SEM images of the tensile fracture surface of the 8-$RC_2B_8$ sample (d) (◆: NR/*h*BN layer; ★: NR/CNT layer). The arrows in the images point to the position of the interface between two adjacent layers.

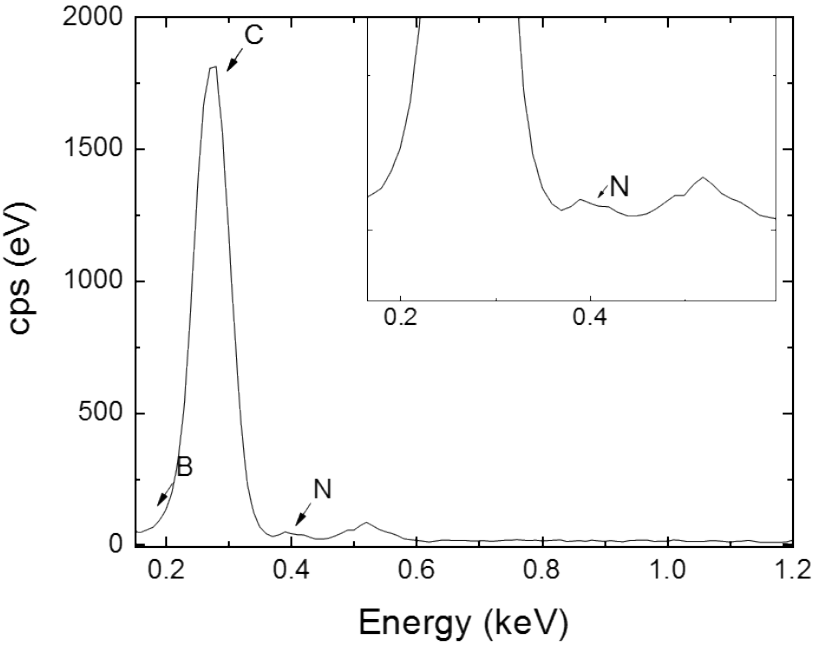


**Figure S3**. Energy dispersive spectrum for 8-$RC_8B_8$ composite.

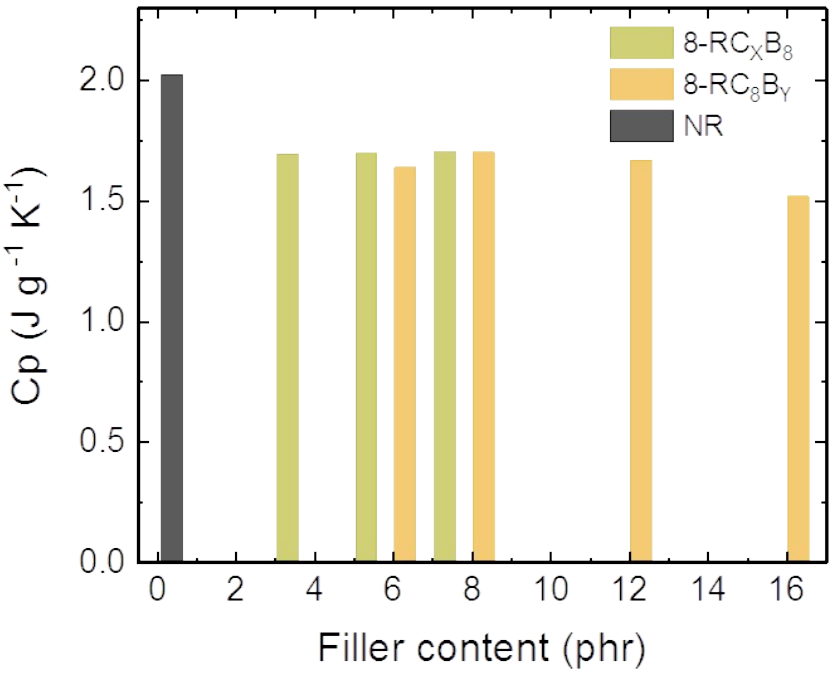


**Figure S4**. Specific heat capacity of RCB composites at 25 °C

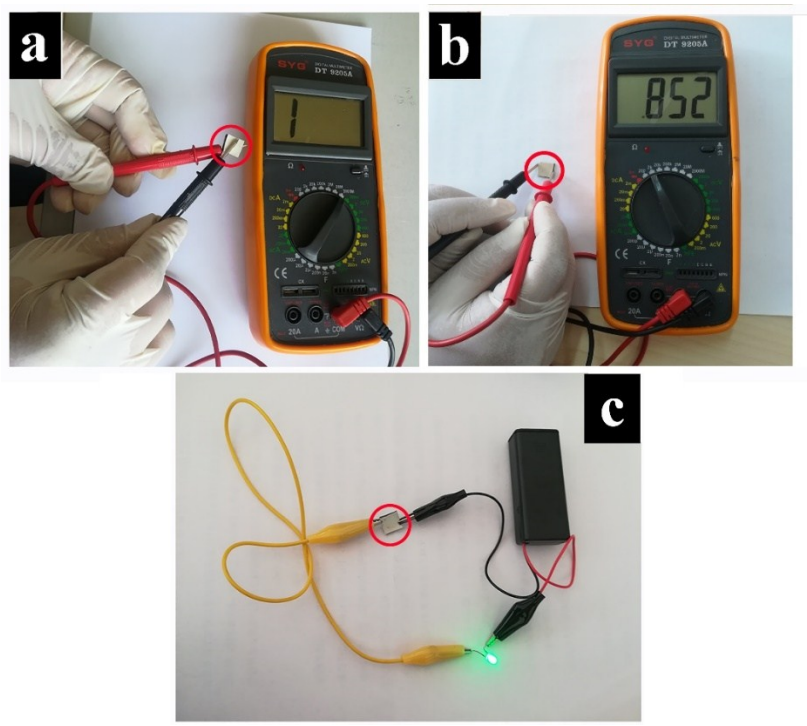


**Figure S5**. Electrical resistance measurement of 8-$RC_8B_{12}$ composite in through-plane direction (a) and in-plane direction (b); and the image of electronic circuit design (c).

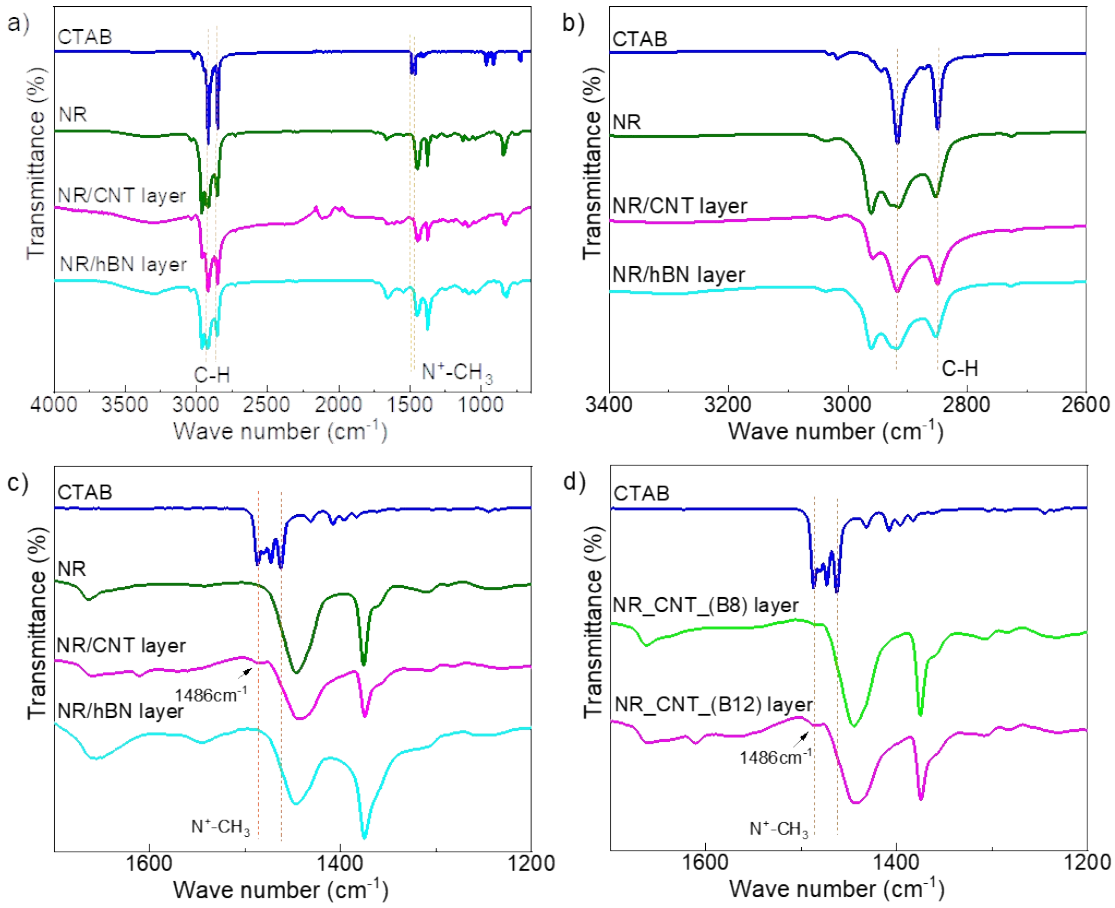


**Figure S6**. Fourier transform infrared spectra of CTAB, NR, NR/CNT layer and NR/*h*BN layer of the sample 8-RC$_8$B$_{12}$: a) from 400 cm$^{-1}$ to 4000 cm$^{-1}$; b) from 2600 cm$^{-1}$ to 3400 cm$^{-1}$; c) from 1200 cm$^{-1}$ to 1700 cm$^{-1}$. d) FTIR spectra of CTAB, NR/CNT layer of the sample 8-RC$_8$B$_8$ and sample 8-RC$_8$B$_{12}$.

The reduction of the electrical conductivity for RCB composites by increasing the amount of *h*BN can be ascribed to the effect of cetyltrimethylammonium bromide (CTAB) surfactant, which adhering onto the surface of CNT limits the filler-filler contacts and affects the conductive pathways. In details, the reduction of the electrical conductivity is attributed to the CTAB content that remains in NR/CNT layers during the filtration process. Indeed, since the NR/CNT dispersion is always filtered as first, during filtration, the surfactant coming from the NR/*h*BN dispersions (the ratio between the surfactant and the filler is fixed equal to 1:1) permeates into the NR/CNT layers and deposits onto the surface of the CNTs contributing to reduce the tunnelling electron transport. The higher is the *h*BN content, the higher is the content of

surfactants that permeates through the CNTs layers and potentially adhere to the CNTs surfaces.

To confirm the aforementioned discussion, FTIR analyses have been performed on the two layers of 8-$RC_8B_{12}$ and 8-$RC_8B_8$ composites, *i.e.,* the first layer with only CNTs (NR/CNT layer) and the last layer containing hBN (NR/*h*BN layer). The FTIR results are shown in **Figure S6**. The pristine NR and CTAB present adsorption bands in a similar region. In fact, ATR-FTIR spectrum of the NR exhibits characteristic absorption bands of $CH_3$ asymmetric, $CH_2$ asymmetric and $CH_2$ symmetric stretching at 2961, 2920 and 2853 $cm^{-1}$, respectively. The bands at 1446 $cm^{-1}$ and 1377 $cm^{-1}$ are assigned to the $CH_3$ and $CH_2$ deformations, respectively, and the band at 837 $cm^{-1}$ is related to the CH out-of-plane deformation. The spectrum of CTAB shows two sharp peaks at 2918 and 2850 $cm^{-1}$ related to the C-H stretching vibration of methyl and methylene groups. The peaks at 1487, 1473, 1463 and 1431 $cm^{-1}$ correspond to symmetric and asymmetric C-H scissoring vibrations of $N^+$-$CH_3$ moiety, while the bands at 960 $cm^{-1}$ are related to the C-$N^+$ stretching,demonstrating the presence of CTAB in the samples.

Although the NR and CTAB show adsorption bands in similar regions and the quantity of CTAB, which remain in the RCB samples, is very low after filtration, it is possible to observe some differences by comparing FTIR spectra of the NR/CNT and NR/*h*BN layers for the same composites and also by comparing different composites. The spectrum of the NR/hBN layer shows the adsorption bands at 2961, 2920 and 2853 $cm^{-1}$ with the same relative intensities of those observed in the spectrum of the pure NR. Instead, different relative intensities of these three peaks are observed in the spectrum of the NR/CNT layer. In particular, the peak at 2918 $cm^{-1}$ is more intense than the peak at 2850 $cm^{-1}$.Both peaks are sharper than in the case of the same adsorption bands shown by the NR and the NR/hBN layer. The increase of the peak's intensity at 2918 $cm^{-1}$ can be attributed to the presence of the surfactant.

Moreover, in the spectrum of the NR/CNT layers is observed the appearance of a shoulder at 1486 $cm^{-1}$ related to the (-$N^+$-$CH_3$) moieties of the CTAB, which are not present in the spectra of both the pristine NR and the NR/*h*BN layer (that means the

CTAB is leached from the NR/hBN layer but it remains onto the surface of CNTs). Therefore, from FTIR analysis it is possible to conclude that the quantity of CTAB in the NR/CNT layers is higher than that present in the NR/*h*BN layers.

At the same time, the FTIR results confirm that the quantity of CTAB presents in the layer with CNTs depends on the content of surfactant in the *h*BN layer. The higher is the content of CTAB in the *h*BN layer, the higher is the content which is left adhering onto the CNTs surfaces. In particular, **Figure S6d** reports a comparison between spectra of NR/CNT layers of samples with different content of *h*BN. It is evident that the intensity of the shoulder at 1486 $cm^{-1}$ is higher in the spectrum of the NR/CNT layer of the sample 8-$RC_8B_{12}$ than in the spectrum of the NR/CNT layer of the sample 8-$RC_8B_8$. This demonstrates that the quantity of CTAB in the layers containing CNTs increases with the amount of *h*BN filler in the RCB composites, and thus it contributes to reducing the electrical conductivity values of materials containing 8 phr of CNT with content of *h*BN higher than 8 phr.

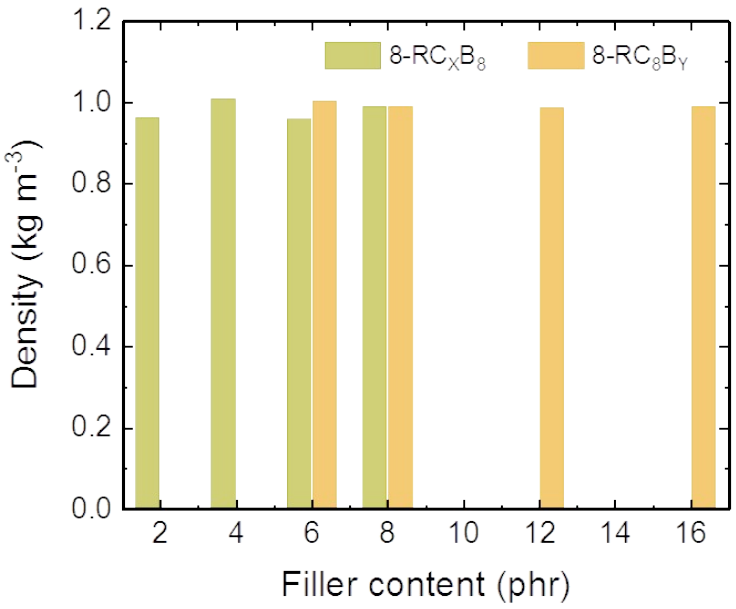


**Figure S7.** Effect of filler content on the density of RCB composites

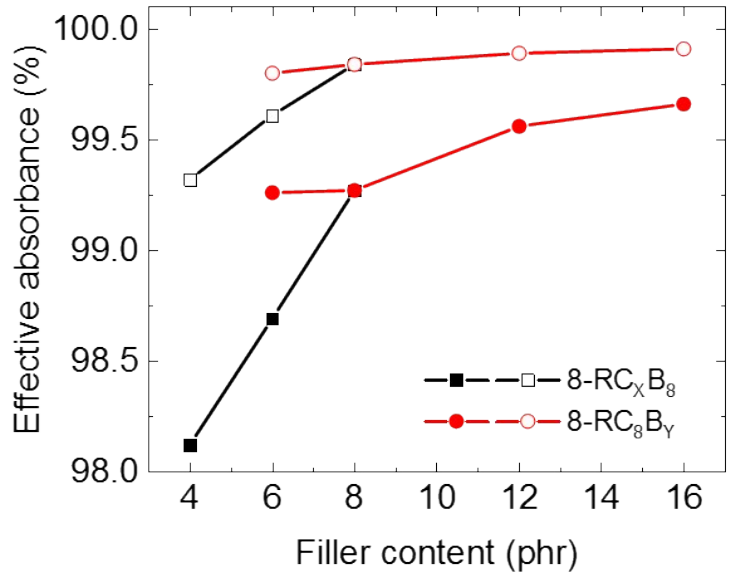


**Figure S8.** Effective absorbance of 8-RCxBy composites (solid symbol: EM waves enter into samples from NR/CNT layer; hollow symbol: EM waves enter into samples from NR/*h*BN layer)

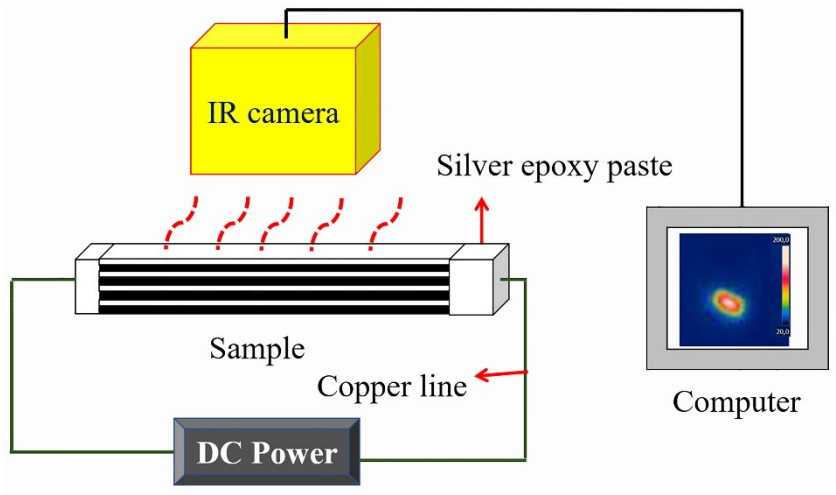


**Figure S9**. Schematic illustration of surface temperature measured by IR camera under fixed voltage.

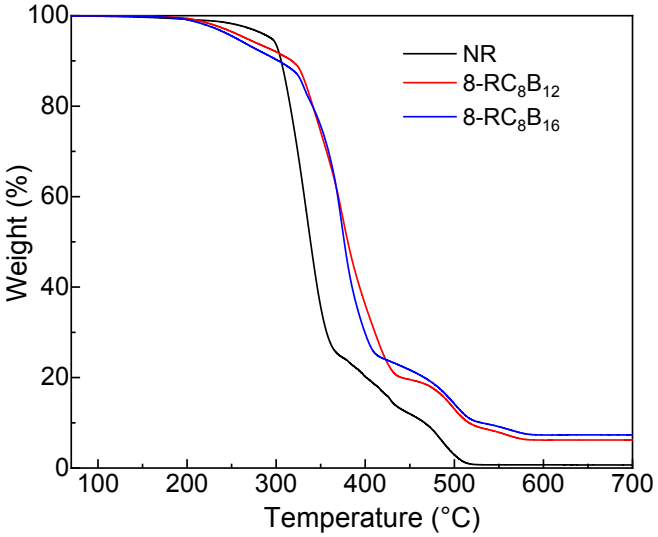


**Figure S10.** Thermogravimetric curves of NR and RCB composites

## References

[S1] Y. Zhan, M. Oliviero, J. Wang, A. Sorrentino, G. G. Buonocore, L. Sorrentino, M. Lavorgna, H. Xia, S. Iannace, Nanoscale, 2019, 11, 1011-1020

[S2] L-C. Jia, D-X. Yan, Y. Yang, D. Zhou, C.H. Cui, E. Bianco, J. Lou, R. Vajtai, B. Li, P. M. Ajayan and Z-M. Li, Adv. Mater. Technol., 2017, 2, 1700078

[S3] J. Abraham, M. Arif P, P. Xavier, S. Bose, S. C. George, N. Kalarikkal and S. Thomas, Polymer, 2017, 112, 102-115.

[S4] N. Joseph, C. Janardhanan and M.T. Sebastian, Compos. Sci. Technol., 2014, 101, 139-144.

[S5] P. Zhao, L. Li, Y. Luo, Z. Lv, K. Xu, S. Li, J. Zhong, Z. Wang and Z. Peng, Compos. Part B, 2016, 99, 216-223.

[S6] I. Kong, S.H. Ahmad, M.H. Abdullah, D. Hui, A.N. Yusoff and D. Puryanti, J. Magn. Magn. Mater., 2010, 322, 3401-3409.

[S7] A.A. Al-Ghamdi, O.A. Al-Hartomy, F. R. Al-Solamy, N. Dishovsky, M.

Mihaylov, N. Atanasov, G. Atanasova and D. Nihtianova, J. Polym. Res., 2016, 23, 180.

[S8] L.C. Jia, Y.K. Li and D.X. Yan, Carbon, 2017, 121, 267-27

[S9] Y. Zhan, J. Wang, K. Zhang, Y. Li, Y. Meng, N. Yan, W. Wei, F. Peng, H. Xia, Chem. Eng. J., 2018, 344,184-193

[S10] J. An, Y.G. Jeong, Eur. Polym. J., 2013, 49, 1322–1330.

[S11] Y.G. Jeong, J. An, Compos. Part A, 2014, 56, 1–7.

[S12] J. Yan, Y.G. Jeong, Compos. Sci. Technol., 2015, 106, 134–140.